Dielectric Waveguide-Based Leaky-Wave Antenna at 212 GHz

Ananjan Basu and Tatsuo Itoh, *Fellow, IEEE*

***Abstract*—The design and fabrication of a leaky-wave antenna at 212 GHz with a dielectric waveguide as the guiding structure is described and some measured results are presented. At this frequency, previously reported approaches for fabricating such an antenna present certain difficulties, which have been overcome using some innovations. This antenna is expected to be useful for radiometry and, consequently should have small beamwidth, high efficiency, and large beam scanning with frequency. It is shown how these can be achieved.**

***Index Terms*—Leaky-wave antennas.**

I. Introduction

THE antenna described here was developed for a specific airborne imaging radiometer, although it can potentially be used for other systems as well such as collision avoidance radars and weapons detection systems. An imaging radiometer, however, has already been built and tested by Thermo-Trex Corp., San Diego, CA, using slotted waveguides for antennas [1]. The beam scanning of a slotted waveguide with frequency is quite small and the dielectric waveguide is a low-loss alternative that has a larger scan. To clarify the requirements on the antenna, a brief description of the imaging system is given.

The imager uses a number of frequency scanned leaky-wave antennas, as shown in Fig. 1, to form a planar array. Broad-band thermal noise is incident on this array from the surroundings with different intensities from different directions. The noise power at the output of any of the antennas at a *particular frequency* is proportional to the noise power incident from the *corresponding direction*, in the y–z plane. Also, at a particular frequency, if we look at the power in the portion of the signal that has a *particular progressive phase shift* from one antenna to the next, we get the power incident from the corresponding direction in the x–y plane. So the noise output (over some band) from the antennas contains the information necessary to form a two-dimensional image of the surroundings. In practice, this information is extracted from the antenna output using an electro-optic modulator [1] following a down-converter since signal processing is not practical at frequencies as high as 212 GHz (or even 94 GHz) where the antenna is small enough to be useful. This system (since it uses millimeter waves) has good penetrating power in poor weather like all millimeter wave imagers and, in addition (since a planar antenna is used), takes up *little volume* unlike the focal plane array, for instance.

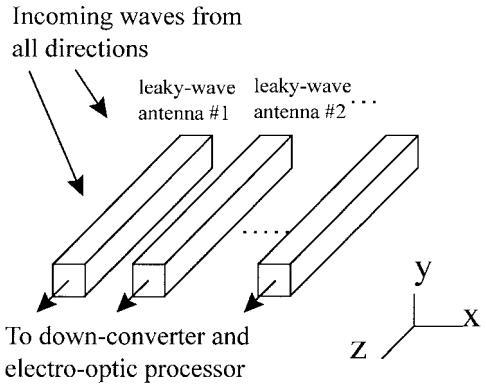

Fig. 1. Schematic diagram of imaging array.

From the above description, some requirements on the antenna begin to emerge. First, the beamwidth has to be very small to maintain a reasonable resolution at distances around 1 km or more. From previous experience, the beamwidth aimed for was 0.3°. This means that the antenna has to be electrically very long, hence, frequency has to be very high to maintain a reasonable size. For this beamwidth, a length of 30 cm at 212 GHz is a reasonable figure. Lengths or frequencies much greater than this are impractical, at least with current supporting technology.

The other important parameters are scan range, and efficiency. The variation of scanning angle over the band of interest is of course dependent on the bandwidth and can be very large in principle. However, the output of the antennas is down-converted to X band and, at that frequency, a bandwidth of 12 GHz is about the maximum that can be expected. Translated to a center frequency of 212 GHz where atmospheric absorption is low, this defines the bandwidth of interest to be 206–218 GHz. A slotted waveguide like the one shown in Fig. 2 gives a scan range of 5.5° over this range. To be useful, a dielectric waveguide-based antenna has to result in a scan range substantially greater.

The variation of main beam direction with frequency (beam scanning) is greatly enhanced by an increase in the *normalized* propagation constant $(\beta/k0)$. Dielectric waveguides using dielectrics with large ε_r($\sim$10 in practice) exhibit this effect to a high degree, especially for a particular frequency band depending on the geometry [2]. Among the materials commonly available, sapphire and silicon are known to have low dielectric losses up to these high millimeter wave frequencies [2]. Sapphire, being very hard, is difficult to form into thin

Manuscript received March 11, 1997; revised July 17, 1998. This work was supported and initiated by Thermo-trex Corp., San Diego, CA.

The authors are with the Electrical Engineering Department, University of California, Los Angeles, CA 90095 USA.

Publisher Item Identifier S 0018-926X(98)08887-5.

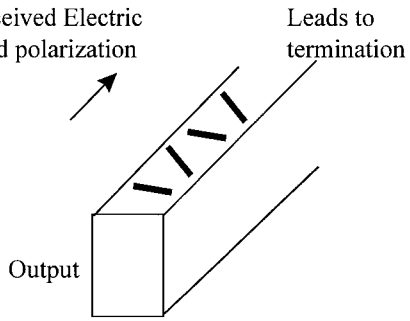

Fig. 2. Slotted waveguide with narrow wall slots.

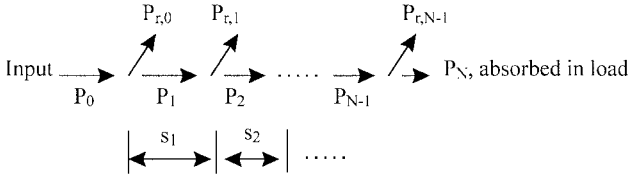

Fig. 3. Model of leaky-wave antenna in transmitting mode.

rods and high resistivity silicon ($\rho \sim 10^4 \Omega$ cm) was chosen as the waveguiding medium. Other materials which might prove useful are germanium ($\varepsilon_r = 15$) and certain artificial ceramics with $\varepsilon_r > 20$. However, few data are available on the dielectric losses of these materials above 200 GHz.

Simple calculations based on the effective dielectric constant (EDC) approach [3] indicate that a silicon waveguide can, in principle, give a scan range of 20°. This was taken as the figure to aim for, although it was subsequently found to be very difficult to realize in practice.

The antenna efficiency is the last important parameter that should be maximized. This is primarily determined by the antenna loss (both guide loss and loss in the transition to rectangular waveguide), for a "correctly designed" (to be clarified later) antenna. It is difficult to specify a particular value, but it has been observed that the imager performance is seriously impaired by efficiencies lower than 50%.

From the preceding discussion, the parameters aimed for can be summarized as follows:

frequency range: 206–218 GHz;
scan range aimed for: 20°;
beamwidth: 0.3°;
length: 30 cm;
efficiency aimed for: 50%.

II. Design Issues

A. Array Considerations

A simple model of a periodically perturbed leaky-wave antenna is shown in Fig. 3. This assumes that the power that is incident on each perturbation is partially radiated and partially transmitted onward through the guide. The power remaining in the guide after the last perturbing element is assumed to be absorbed in a load. This neglects reflections, higher modes, phase shift of propagating wave at perturbations, etc. This simple model turns out to be very useful in practice and the approximations are reasonable for a long antenna with many small perturbations [4]. The following equations relating to this model are basically the ones encountered in linear array theory, with minor generalizations. These are, however, essential in order to go from design specifications to physical dimensions and a brief description is appropriate.

The symbols used are as follows.

P_i	Power in the guide incident on the ith perturbation $(i = 0 \cdots N-1)$. P_0 is the power input to the antenna and P_N is the power absorbed in the termination.
$P_{r,i}$	Power radiated from the ith perturbation.
$C_i = P_{r,i}/P_i$	This implicitly neglects coupling between perturbations. C_i is related to the geometry of the ith perturbation and this relation needs to be known. C_i is subsequently referred to as the radiation coupling coefficient.
α	Field attenuation constant for losses in the waveguide (*not* the loss due to radiation at perturbations), in nepers/m.
s_i	Separation between ith and $(i-1)$th perturbations. s_0 is, of course, not defined. If the patches are equally spaced, with spacing "s" (which is almost always the case) the distance of the ith patch from the first $(i = 0)$, is $(i \cdot s)$ and this can replace the expression $(s_1 + \cdots + s_i)$ in the following.

The two important equations of interest are

$$P_i = P_{i-1}(1 - C_{i-1})e^{-2\alpha s_i} \tag{1}$$

$$|E_{\text{far}}| = \left| \sum_{i=0}^{N-1} E_i \exp(-j(\beta - k_0 \sin\theta)(s_1 + s_2 + \cdots + s_i)) \right|. \tag{2}$$

Here, E_i is the far field of the ith radiating element and $E_i \propto \sqrt{P_{r,i}}$, with $P_{r,i}$ being determined by C_i.

E_{far} is the radiated electric field of the antenna in the far-field zone.

Usually, we wish to make $\sqrt{P_{r,i}}$ proportional to some given $f(i)$, generally a constant for "uniform aperture illumination." So, given $f(i)$ we have to calculate $C_0 \ldots C_{N-1}$.

Let P_N be the portion of input power finally dumped into the load and define "x" by

$$P_N = P_{N-1}(1 - C_{N-1}) = xP_0. \tag{3}$$

The value of "x" can be specified as a design parameter, typically $\sim$0.01.

The important design requirement is

$$P_{r,i} = f^2(i) \tag{4}$$

where $f(i)$ is a given function (typically constant). A normalization constant can always be included, which we have assumed to be one. The above relations are sufficient for determining $C_0 \cdots C_{N-1}$ as follows.

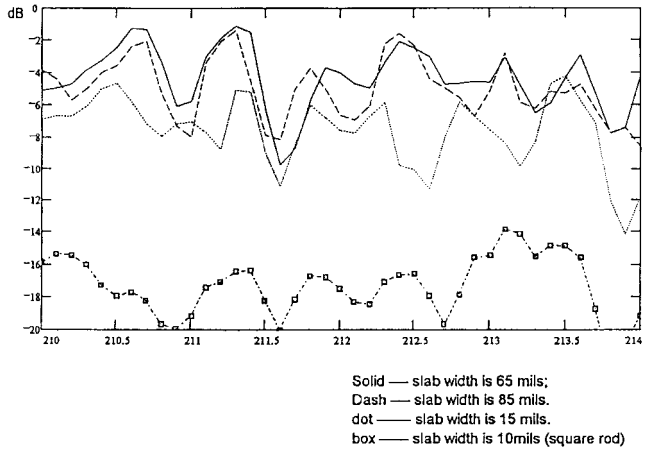

Fig. 4. Insertion loss of different widths of silicon rod, 12 mils thick, 2 in long.

Starting from (1) and using (3) and (4), we can arrive at (5), shown at the bottom of the page. This forms the starting point in order to recursively obtain C_i.

$C_i = f^2(i)/P_i$; then use (1) to obtain P_{i+1}; P_0 is found from (5) to start the recursion.

Finally, if we had a relation between C_i and the geometry of the perturbation, the design for achieving a given $f(i)$ would be complete (what was earlier referred to as a "correct design"). On the other hand, without following a procedure such as the one just outlined, either an undesirable aperture illumination will result or an excess of power will be wasted in the termination.

For a 30-cm-long antenna with element spacing $= 0.55$ mm (which gives a main beam around 20° at 212 GHz), for $x = 0.05$ and guide loss of 0.5 dB/in, the radiation coupling coefficients should have values from 0.0006 to 0.01, to achieve uniform illumination. So, the perturbation scheme should be capable of realizing this range of C_i.

In principle, a relation between the radiation coupling coefficients and the geometry can be obtained through numerical analysis, for example, by using the finite-element-method-based software package HFSS, but the accuracy of such results is questionable, mainly because of nonidealities in fabrication of the small structures involved. It is better to obtain experimental data relating C_i to the geometry, as will be demonstrated in a later section.

B. Transition

This antenna, like most components, needs a transition to standard waveguide. The simplest possible transition is formed by simply inserting the dielectric rod into the metal waveguide. This works satisfactorily at W band, as has been shown in [2]. Around 212 GHz however, a single-mode silicon waveguide (10 mils × 10 mils wide), with the ends inserted into the waveguide mouth shows an extremely high insertion loss. The loss goes down sharply as the width of the rod is increased from 10 to 15 mils, and is roughly constant when the width is increased beyond 30 mils; a satisfactory explanation has not yet been found for this observation. The variation of loss with frequency for different widths is shown in Fig. 4. Of course, silicon rods 15 mils and greater in width are multimode waveguides.

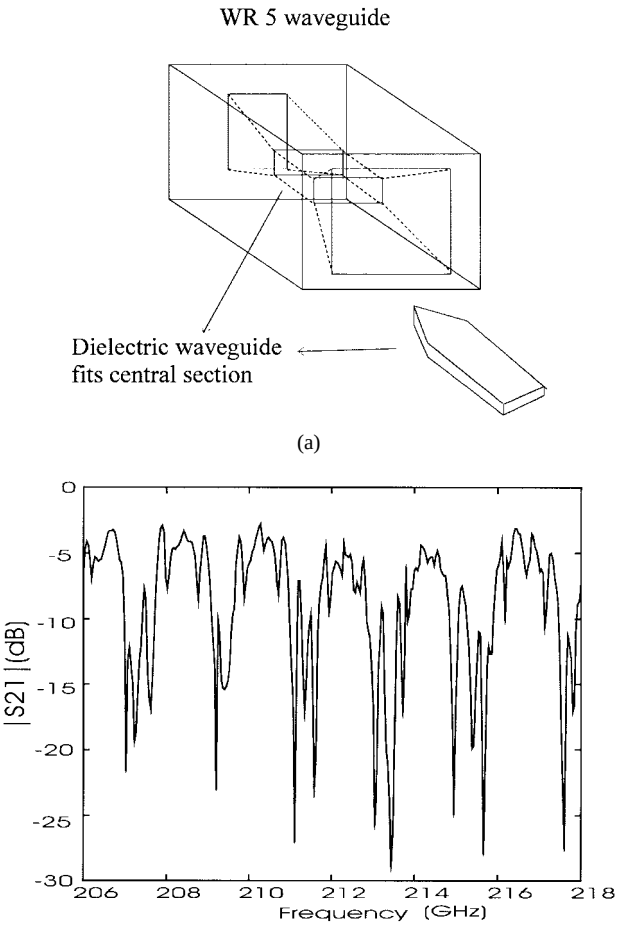

Fig. 5. (a) Structure of an elaborate transition from rectangular metallic to dielectric waveguide. (b) Insertion loss for this transition in back to back configuration.

The insertion loss shown in Fig. 4, is still quite high, although we cannot separate the guide loss and transition loss from these data. An attempt was made to build a better transition, following [5]. The structure is shown in Fig. 5(a), and the insertion loss in Fig. 5(b). It can be seen that this type of transition is not suitable for multimode dielectric guides since there is hardly any bandwidth between the dips.

A better way of improving the transition is to taper the ends of the silicon rod that go inside the waveguides. This taper can be either "one way," in which only one pair of opposite faces

$$P_0 = \frac{f^2(0) + e^{2\alpha s_1} f^2(1) + \cdots + e^{2\alpha(s_1+s_2+\cdots+s_{N-1})} f^2(N-1)}{1 - x e^{2\alpha(s_1+s_2+\cdots+s_{N-1})}} \tag{5}$$

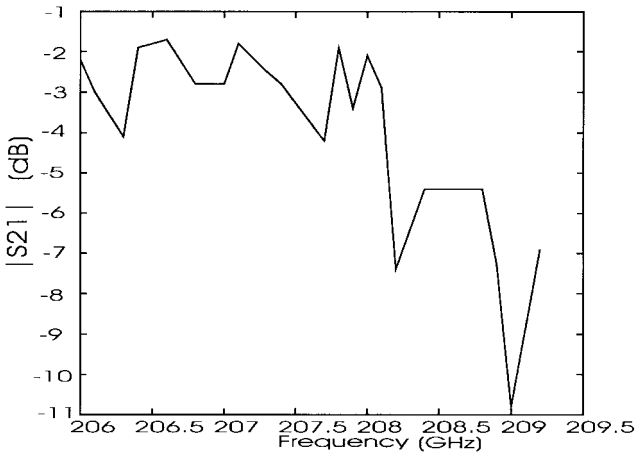

(a)

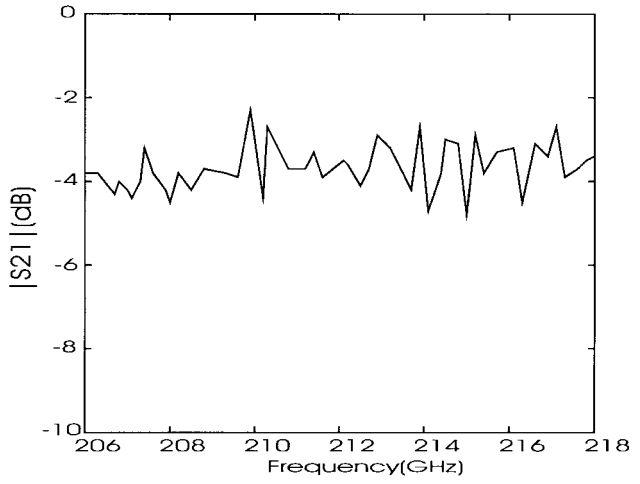

(b)

Fig. 6. (a) Insertion loss of one-way tapered transition. (b) Insertion loss of two-way tapered transition.

is tapered, or "two way," in which both pairs of opposite faces are tapered, giving a pyramidal end to the silicon waveguide. The insertion losses for these two cases are shown in Fig. 6(a) and (b). As we can see, the response is reasonably flat over the frequency band of interest only for the two-way taper. In addition, the two-way tapered transition has an important effect on the radiation pattern of the antenna, which is discussed next.

C. Effect of Higher Modes

A silicon waveguide 35 mil $\times$ 12 mil in cross section supports many modes around 212 GHz. Specifically, for the symmetry shown in Fig. 7, the first three modes have the normalized propagation constants (β/k_0): 2.98, 2.4, 2.1. These modes can roughly be classified as $E_x^{1,1}$, $E_x^{1,2}$, and $E_x^{3,1}$ (i.e., electric field is dominantly x polarized), where superscripts denote the number of peaks along x and y (disregarding the discontinuity of E_x at the vertical junctions between silicon and teflon). It can be seen that there are many modes with propagation constants not differing widely. This has the following consequences.

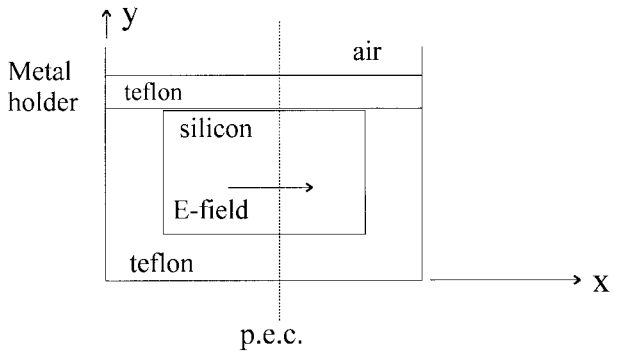

Fig. 7. Assumed symmetry in the fields.

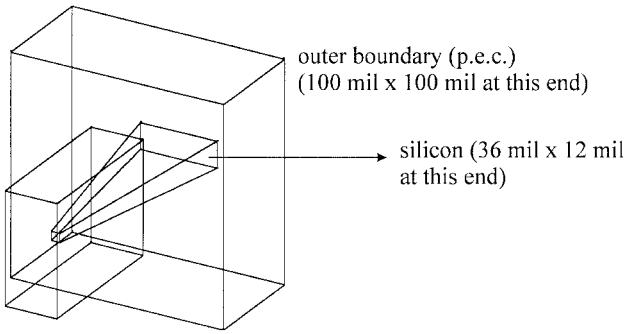

Fig. 8. Transition structure simulated by HFSS. The metal waveguide port is shown at the left and the dielectric waveguide port on the right. Shielding is added for simplicity.

The main beam of a leaky-wave antenna (with uniformly spaced elements) points in a direction that is off broadside by an angle θ, where $\theta = \sin^{-1}(\beta/k_0 - n\lambda_0/s)$ and "s" (the spacing) is so chosen that only $n = 1$ gives a real θ. In addition, we can try to choose a spacing such that only the β for the dominant mode gives a real θ, but this usually results in a main beam close to end fire and large beamwidth, which is undesirable. So, for different modes having different β, we have different main beam directions; that is, such an antenna may produce multiple "main" beams. However, the higher modes *do not couple into the metal waveguide via the tapered transition*. This was verified by simulating a transition structure using HFSS. The structure simulated is shown in Fig. 8. The simulated multimode S parameters of this structure are

Mode 1 input, mode 1 output: 0.9912
Mode 1 input, mode 2 output: 0.0138
Mode 1 input, mode 3 output: 0.0055
Mode 1 input, mode 4 output: 0.0038.
.....

Here, input is the metal waveguide and output is the dielectric waveguide. For computational ease, a perfect electric conductor (PEC) boundary is used a reasonable distance away from the dielectric, but all the fields have been seen to be practically zero there so an open boundary will give almost identical results. These numbers clearly indicate that while the received signal in this antenna may propagate in a number of modes, only the dominant mode couples into the metal waveguide output. So, an overmoded waveguide does not create any problems in this respect.

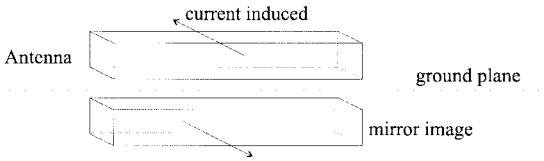

Fig. 9. Mirror image due to ground plane.

D. Element Factor

A perturbation on a dielectric waveguide has its own radiation pattern: the element factor for the leaky-wave antenna. For a narrow main beam, obtained with a large number of elements, this is not important provided one condition is satisfied. When there is a ground plane under the dielectric waveguide, each perturbation gives rise to a mirror image, as shown in Fig. 9. Due to this, the array pattern should be multiplied by the term $\sin(k_0 h \cos\theta)$. This term is slowly varying compared to the array factor, unless *it goes to zero for some* θ. It is necessary to ensure that such nulls do not coincide with the main beam direction *for any frequency* in the band of interest.

Here we have assumed that the radiation from the image travels through free-space, which is a gross approximation. A better estimation for the element pattern can be obtained by calculating the element pattern for an infinitesimal current element on (or inside) a layered dielectric structure obtained by replacing the dielectric rod by a layer with an appropriate effective dielectric constant, following Mittra and Kastner [6]. Since the far field is related to the Fourier transform of the near field, the radiation pattern can be easily calculated from the spectral-domain Green's function for this structure. The calculated radiation pattern for a fairly realistic structure that is shown in Fig. 10(a), is shown in Fig. 10(b). This still shows a null at 218 GHz, establishing that care has to be taken while choosing "h."

To summarize, the principal design issues which have to be taken care of are:

1) there should not be spurious "main" beams due to multimoding;
2) nulls of the element pattern should not coincide with the main beam direction of the array for any frequency in the band of interest;
3) the desired aperture illumination (uniform, for this application) should be achieved without loss of efficiency (that is, in transmitting mode, as much input power should be radiated out as possible with a minimum of losses in the terminating load or in the transition).

It will be shown next that the first two objectives are achieved in practice. The realization of a uniform aperture illumination, and high efficiency are essentially consequences of an accurate measurement of the radiation coupling coefficients and a procedure for doing this is demonstrated on a simplified antenna structure.

III. Experiments

A. Fabrication

Due to the small dimensions involved, each part of the antenna had to be fabricated with great care. Perfecting the processes involved was actually the most time-consuming part in the development of this antenna. First, a test antenna, with a 2 in silicon rod of which 0.5 in was covered by 20 perturbing elements (later referred to as the 0.5-in-long antenna), then a 5.5-in-long antenna and a 10.5-in antenna (with perturbations covering the full length for these two) were fabricated. The different parts of the antenna areas follows.

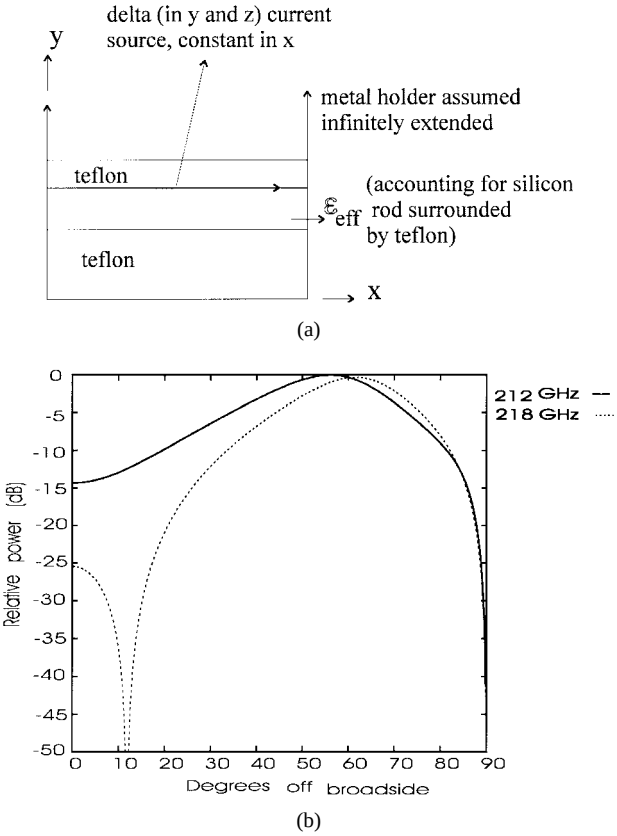

Fig. 10. (a) Simplified structure for approximate evaluation of radiation pattern. (b) Radiation pattern of the structure in (a).

1) A metal holder with detachable waveguide flanges at both ends.
2) A slotted teflon or quartz strip made to fit in the holder for supporting the silicon rod.
3) A silicon rod of rectangular cross section 35 mils $\times$ 12 mils with tapered ends.
4) A teflon sheet with printed copper patches for radiating elements.

Each of these merits a brief description to bring out the novel features in its construction.

1) Holder: Cross-sections of two holders which have been used are shown in Fig. 11(a) and a photograph of the first is shown in Fig. 11(b). The second structure, with the silicon sandwiched between two teflon sheets gives a more reliable contact between the radiating patches and the silicon rod. The alignment of the silicon rod is a little difficult for short antennas, but for antennas longer than 5 in it is satisfactory. The flaring out of the holder in the transverse plane serves to increase the gain in this plane. The structure is similar in appearance to the trapped image dielectric waveguide [7], but functionally the guide is closest to the basic rectangular

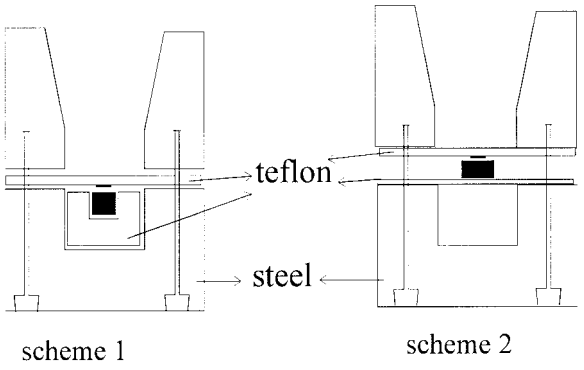

(a)

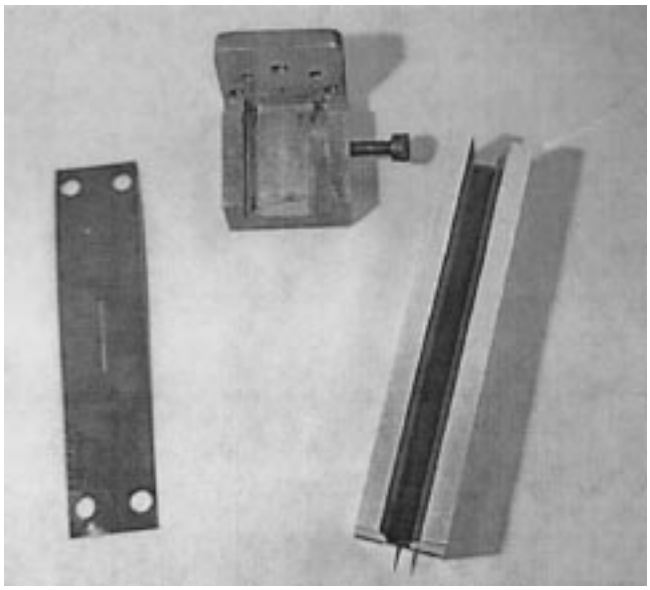

(b)

Fig. 11. (a) Cross sections of two holders. (b) Photograph of 2–in-long test holder, waveguide adapter, and a sample teflon sheet with printed perturbations.

dielectric waveguide, the teflon and the holder serving merely as supports as far as the waveguiding aspect is concerned. In particular, the structure avoids ground-plane conductor losses which can be very large for a 200-wavelengths-long antenna. The flared portion and the base are made from separate pieces held together by screws that also serve to align the teflon sheet with the printed radiating elements. The holder is made out of stainless steel since it has to be absolutely straight and softer materials like brass or aluminum, although easier to work on, tend to warp slightly for long structures like this.

The holder fits to brass end pieces containing built-in G-band waveguide flanges, which accommodate the tapered silicon rod on the antenna side and connect to a standard G-band waveguide on the outer side. The waveguide opening is formed by wire electrical discharge machining (EDM).

2) Support: For the 0.5 in antenna, a grooved strip machined from teflon was used to hold the silicon rod. For the 10.5-in-long antenna, quartz was also tried as a support material, as the dimensioning can be more precisely achieved with a dicing saw. The cross section of such a quartz support is shown in Fig. 12. However, as will be shown in the next section, this technique was not successful for the longer antennas.

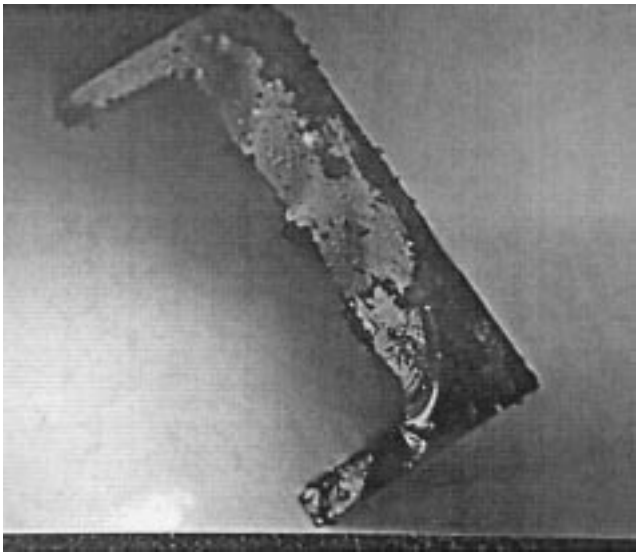

Fig. 12. Microphotograph of quartz holder 50 mils wide.

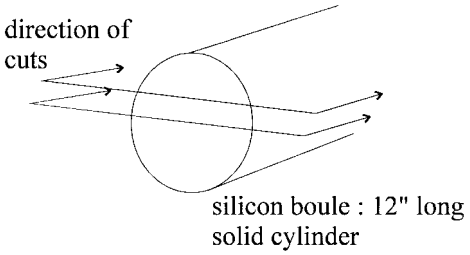

Fig. 13. Slicing of silicon boule to obtain thin plates 12 in long.

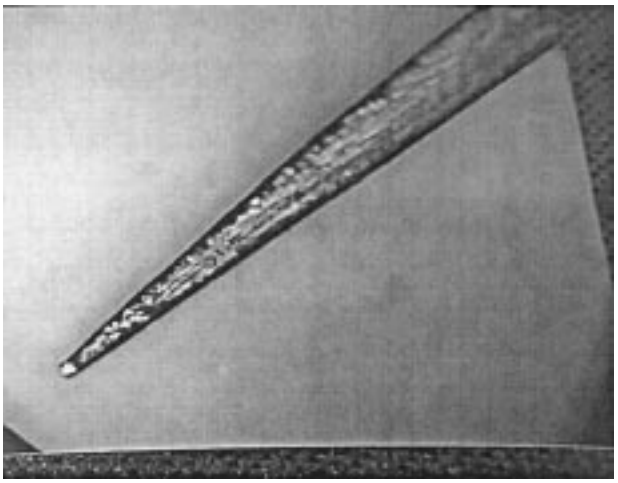

Fig. 14. Microphotograph of a double-tapered silicon rod. A hair is shown in the bottom left corner for comparison.

3) Silicon Rods: To obtain silicon rods 12 in long and 35 mils $\times$ 12 mils in cross section, first a high-resistivity ($\sim 10^4 \Omega$-cm) silicon boule has to be sliced as shown in Fig. 13 to obtain 12-mil thick plates 12 in long. From this, rods of the required width were cut out using a dicing saw. The slicing of the boule was carried out by Laser Power Optics, San Diego,

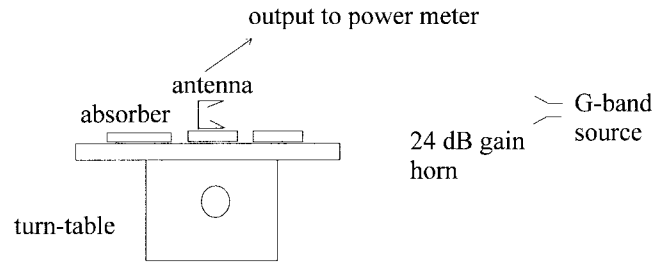

Fig. 15. Simple radiation pattern measurement setup.

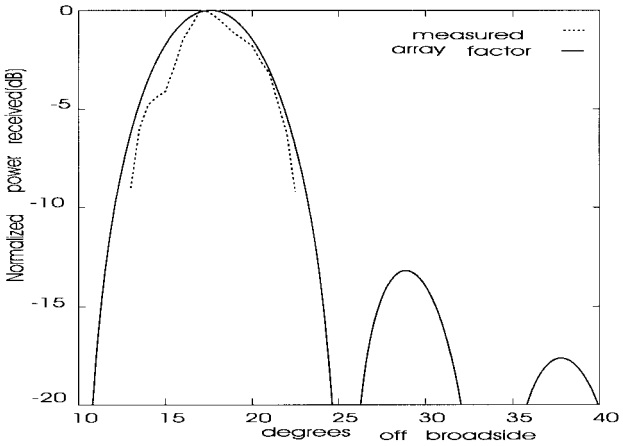

(a)

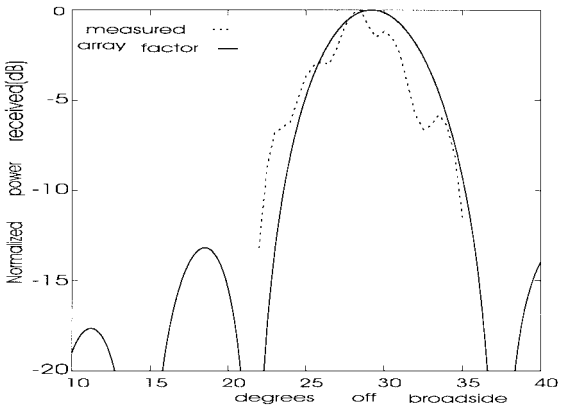

(b)

Fig. 16. (a) Radiation pattern at 206 GHz. (b) Radiation pattern at 218 GHz.

CA. The tapering of the ends was done by grinding on a miniature fine-grained polishing wheel, under a microscope. A microphotograph of such a taper is shown in Fig. 14. Unfortunately, at present the longest available rods are 6 in long instead of the desired 12 in. However, all important features of a 12 in long antenna can be expected to be present in a 6-in-long antenna too. A 0.5-in antenna though, does not show some important effects.

4) Printed Radiators: The teflon sheet used was 5 mils thick, and the thickness of copper was 15 μm. A thicker copper coating (30 μm is commonly used) leads to overetching during photolithography and distorts the shape of the patches.

It should be noticed that an alternative way is to print the patches directly on the silicon. The present structure has been adopted for two reasons:

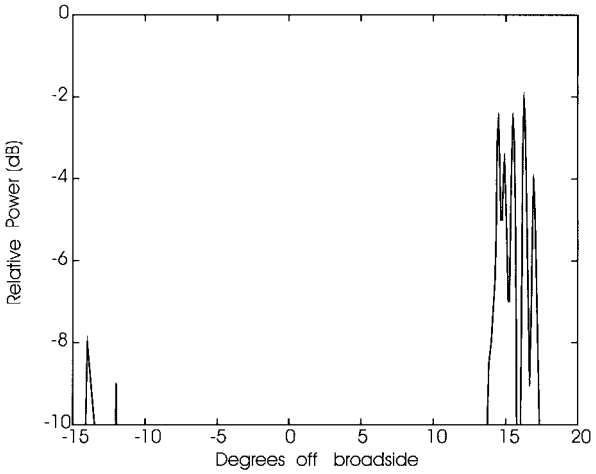

Fig. 17. Radiation pattern of 10.5-in antenna showing problems due to scattering by support.

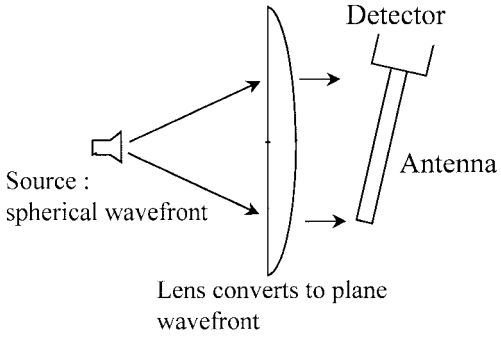

(a)

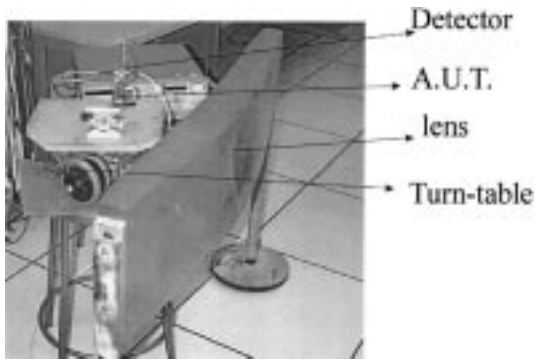

(b)

Fig. 18. (a) Schematic of measurement setup for long antennas. (b) Photograph of a part of the setup.

1) photolithography on easily obtainable copper-coated teflon is easier and cheaper than first coating the fragile silicon rods and the carrying out photolithography on them;
2) the patches can be printed on both sides of the teflon sheet, giving a large range of perturbation strength.

B. Radiation Pattern Measurement

The test antenna fabricated as the first step used a silicon rod 2 in long and had only 20 identical elements with 0.55-mm spacing. The simple test setup is shown in Fig. 15. It

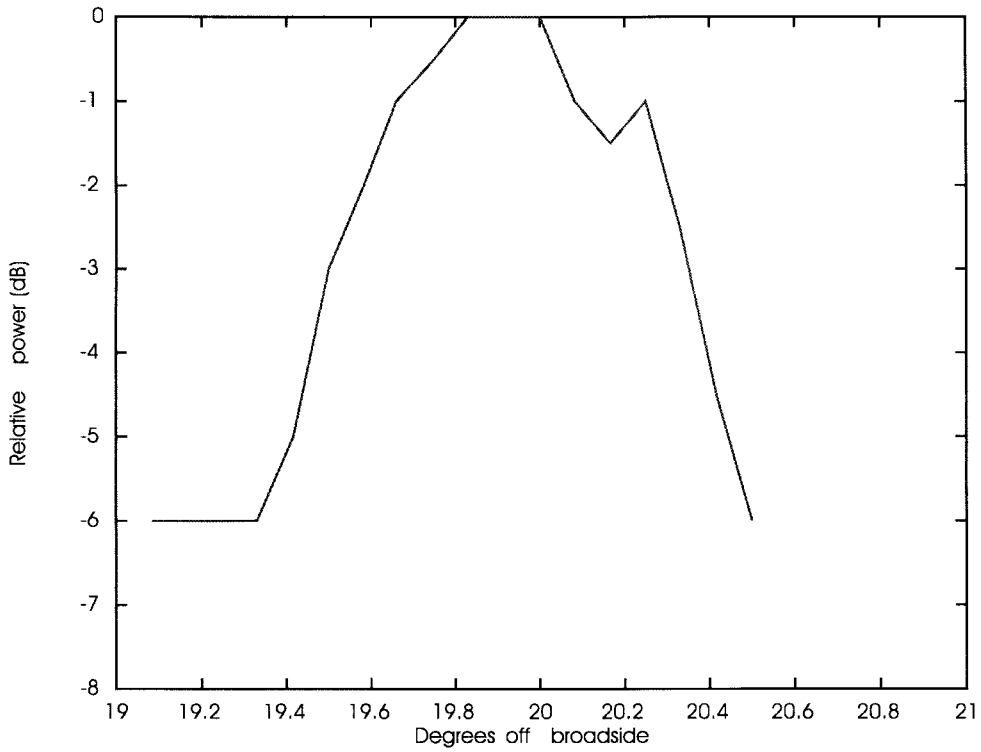

Fig. 19. Measured radiation pattern of 5.5-in antenna at 211 GHz.

can be seen that there are many metallic parts that can cause spurious reflections. Since an anechoic chamber was not available, which was suitable for these frequencies, very accurate measurements were not possible. The radiation patterns shown in Fig. 16 do, however, show a reasonable agreement with theory and bring out the two most important features.

1) Beam scanning with frequency: about 11° over the 206–218 GHz band, which is more than twice that obtainable with a slotted waveguide, although substantially less than the 20° aimed for.
2) Absence of spurious "main" beams due to higher modes. The power levels outside the angular extent shown in the plots was below the sensitivity of the power detector, hence, at least 15 dB below the peak.

The peak directive gain is 7–10 dB below a standard (24 dB) horn; that is, 14–17 dB. There is a repeatability problem in measuring this and a more precise assembly (primarily of the transition) is required to measure the gain accurately.

A 10.5-in long antenna using the quartz support (Fig. 12), and perturbations on the top side of the teflon turned out to be completely unsatisfactory, as the radiation pattern (at 206 GHz) of Fig. 17 shows. Similar patterns were observed upon changing to teflon support and/or 5.5-in silicon rods. The problem was due to scattering by imperfections in the support. This did not turn up in the 0.5-in-long antenna, which had strong perturbation by the patches touching the silicon. To solve this problem, the second scheme of Fig. 11(a) was used, and the antenna performance was quite reasonable. Radiation pattern measurement for these longer antennas is more difficult as the far field is a long distance away (around 100 m away for the 10.5-in antenna). So a lens is used to artificially produce a plane wave, as shown in Fig. 18(a) and (b). It is clear that this setup admits many spurious reflections etc. However, from previous measurements on a horn and slotted waveguides, it was seen that the main beam could be measured with reasonable accuracy although sidelobes are badly distorted. A sample radiation pattern is shown in Fig. 19. Due to the low-power levels involved, only a portion of the main beam could be observed. The 3-dB beam width of 0.9° (theoretically calculated for uniform aperture illumination: 0.6°) and beam-pointing angle of 19.8° (theoretically calculated: 20.6°) are fairly close to expectations. Some parameters which could be roughly estimated by comparing with a 24-dB gain horn are:

gain: 25 dB;

efficiency $\approx$ (antenna output power/horn output power)/(antenna aperture area/ horn aperture area) $= 20\%$.

The low value is caused by nonuniform aperture illumination. It should be emphasized that these numbers are only rough estimates and a more sensitive receiver is necessary for precise measurements.

C. Near-Field Probing

For a 12-in-long antenna with $\sim$500 elements, aperture illumination is an important issue and, as discussed earlier, an accurate measurement of the radiation coupling coefficients is required. A probe has been developed [8] to scan the near fields of structures of this type, which is an effective way to measure the radiation coupling coefficients. The procedure is demonstrated on a simpler leaky-wave structure, as shown in Fig. 20.

For this structure, it is has been seen that above each metallized patch there are peaks at which the electric field has a local maximum, and one of these points can be identified by

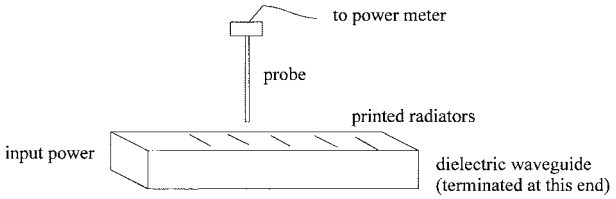

Fig. 20. Probing the fields above the antenna.

moving the probe above the patch with a three-axis precision positioner. This peak electric field decays as we go from one patch to the next as the field in the guide loses power due to radiation. This decay (in decibels) should be constant from one pair of patches to the next (assuming the model of this structure shown earlier is valid). If the decay is "L" dB from one patch to the next (L is negative), then the radiation coupling coefficient for these dimensions can be easily shown to be

$$C = 1 - 10^{L/10}.$$

Here, we have neglected guide loss, which can also be accounted for by repeating the measurement for a (substantially) different element spacing.

The waveguide used for this measurement was a quartz waveguide, 0.4 mm thick and 0.5 mm wide. The metallized patches were 0.5-mm long (the full width of the rod) and 0.2 mm wide. The loss from the first patch to the second was 4 dB and from the second to the third was 6 dB at 212 GHz. An average value of 5 dB indicates that $C = 0.68$ for these dimensions, which is very large, indicating that even thinner patches are required. This is the main reason why a simpler structure such as the one described in [9] cannot be used. Also, a standing wave pattern was observed similar to the one described in [8], hence, reflections are not negligible. However, the possibility of experimental determination of the radiation coupling coefficients is demonstrated.

Characterizing the actual perturbation scheme in the above way is presently being attempted. It is expected that these experiments will lead to the successful fabrication of such an antenna with $<0.3^\circ$ beamwidth.

IV. Conclusion

The design and fabrication of a frequency-scanned leaky-wave antenna for G band using a silicon waveguide is described and it is shown that some of the manufacturing challenges involved can be overcome. Some preliminary results are presented and a procedure outlined for the successful fabrication of such an antenna suitable for an airborne radiometer.

References

[1] J. Lovberg, R.-C. Chou, C. Martin, and J. Galliano, "Advances in real-time millimeter-wave imaging radiometers for avionic synthetic vision," in *Proc. SPIE, Synthetic Vision Veh. Guidance Contr.*, Orlando, FL, Apr. 1995, vol. 2463, pp. 20–27.

[2] S.-M. Wong, "A study on dielectric waveguide and leaky-wave dielectric antenna at millimeter-wave frequencies," M.S. thesis, Elect. Eng. Dept., Univ. California, Los Angeles, 1996.

[3] T. Itoh, "Inverted strip dielectric waveguide for millimeter wave integrated circuits," *IEEE Trans. Microwave Theory Tech.*, vol. MTT-24, pp. 821–827, Nov. 1976.

[4] R. S. Elliott, *Antenna Theory and Design*. Englewood Cliffs, NJ: Prentice-Hall, 1981, ch. 4.

[5] J. A. G. Malherbe, T. N. Trinh, and R. Mittra, "Transition from metal to dielectric waveguide," *Microwave J.*, vol. 23, pp. 71–74, Nov. 1980.

[6] R. Mittra and R. Kastner, "A spectral domain approach for computing the radiation characteristics of a leaky-wave antenna for millimeter waves," *IEEE Trans. Antennas Propagat.*, vol. AP-29, pp. 652–654, July 1981.

[7] T. Itoh and B. Adelseck, "Trapped image guide for millimeter wave circuits," *IEEE Trans. Microwave Theory Tech.*, vol. MTT-28, pp. 1433–1436, Dec. 1980.

[8] A. Basu and T. Itoh, "A new field probing technique for millimeter wave components," in *IEEE MTT-S Int. Microwave Symp. Dig.*, Denver, CO, June 1997, vol. 3, pp. 1667–1670.

[9] K. L. Klohn, R. E. Horn, H. Jacobs, and E. Freibergs, "Silicon waveguide frequency scanning linear array antenna," *IEEE Trans. Microwave Theory Tech.*, vol. MTT-26, pp. 764–773, Oct. 1978.

Ananjan Basu received the B.Tech. and M.Tech. degrees in electrical engineering from the Indian Institute of Technology, Delhi, India, in 1991 and 1993, respectively. He is currently working toward the Ph.D. degree in electrical engineering at the University of California, Los Angeles.

He subsequently held the post of Senior Scientific Officer for one year at the Indian Institute of Technology, Delhi. His area of interest is in millimeter-wave antennas.

Tatsuo Itoh (S'69–M'69–SM'74–F'82) received the Ph.D. degree in electrical engineering from the University of Illinois, Urbana, in 1969.

From September 1966 to April 1976, he was with the Electrical Engineering Department, University of Illinois, Urbana. From April 1976 to August 1977, he was a Senior Research Engineer in the Radio Physics Laboratory, SRI International, Menlo Park, CA. From August 1977 to June 1978, he was an Associate Professor at the University of Kentucky, Lexington. In July 1978, he joined the faculty at The University of Texas at Austin, where he became a Professor of Electrical Engineering in 1981 and Director of the Electrical Engineering Research Laboratory in 1984. During the summer of 1979, he was a Guest Researcher at AEG-Telefunken, Ulm, West Germany. In January 1991 he joined the University of California, Los Angeles as Professor of Electrical Engineering and holder of the TRW Endowed Chair in Microwave and Millimeter Wave Electronics. He is currently Director of Joint Services Electronics Program (JSEP) and is also Director of Multidisciplinary University Research Initiative (MURI) program at UCLA. He was an Honorary Visiting Professor at Nanjin Institute of Technology, China and at Japan Defense Academy. In April 1994, he was appointed as Adjunct Research Officer for Communications Research Laboratory, Ministry of Post and Telecommunication, Japan. He currently holds Visiting Professorship at University of Leeds, United Kingdom and is an External Examiner of Graduate Program of City University of Hong Kong. He has more than 220 journal publications, 380 refereed conference presentations and has written more than 20 books/book chapters in the area of microwaves, millimeter-waves, antennas, and numerical electromagnetics. He has guided 34 students to their doctorates.

Dr. Itoh was selected to hold the Hayden Head Centennial Professorship of Engineering at The University of Texas in September 1983. In September 1984 he was appointed Associate Chairman for Research and Planning of the Electrical and Computer Engineering Department at The University of Texas. He served as the Editor of IEEE Transactions on Microwave Theory and Techniques from 1983 to 1985. He serves on the Administrative Committee of IEEE Microwave Theory and Techniques Society. He was Vice President of the Microwave Theory and Techniques Society in 1989 and President in 1990. He was the Editor-in-Chief of IEEE Microwave and Guided Wave Letters from 1991 through 1994. He was elected as an Honorary Life Member of MTT Society in 1994. He was the Chairman of USNC/URSI Commission D from 1988 to 1990, the Vice Chairman of Commission D of URSI from 1991 to 1993 and Chairman of the same Commission from 1993 to 1996. He is on the Long Range Planning Committee of URSI. He serves on advisory boards and committees of a number of organizations including the National Research Council and the Institute of Mobile and Satellite Communication, Germany. He is a member of the Institute of Electronics and Communication Engineers of Japan and Commissions B and D of USNC/URSI.